Crosslinked poly(vinylbenzyl chloride) with a macromolecular crosslinker for anion exchange membrane fuel cells

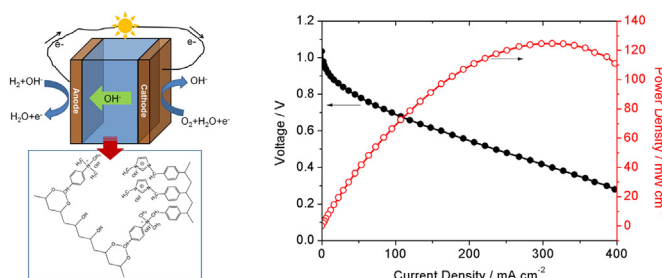Wangting Lu [a, b], Zhi-Gang Shao [a, *], Geng Zhang [a, b], Yun Zhao [a], Baolian Yi [a]

[a] Fuel Cell System and Engineering Group, Dalian Institute of Chemical Physics, Chinese Academy of Sciences, 457 Zhongshan Road, 116023 Dalian, PR China
[b] Graduate School of Chinese Academy of Sciences, 19A Yuquan Road, 100049 Beijing, PR China

HIGHLIGHTS

- Crosslinked AEMs were synthesized by a macromolecular crosslinker.
- Such method combined the advantages of semi-IPN and crosslinking.
- The AEMs exhibited superior OH^- conductivity and suppressed swelling.
- The fuel cell using AEMs herein showed good power output.

GRAPHICAL ABSTRACT

ARTICLE INFO

ABSTRACT

A new material based on crosslinked poly(vinylbenzyl chloride) (PVBC) with a macromolecular crosslinker is synthesized and employed as the membrane for anion exchange membrane fuel cells (AEMFCs). PVBC is used as the hydroxide conducting polymers, while poly(vinyl acetal) (PVAc) containing dimethylamino groups plays the role as macromolecular crosslinker and the supporting matrix simultaneously. Fourier transform infrared (FT-IR) absorption spectra and X-ray photoelectron (XPS) spectra prove successful crosslinking between PVBC and PVAc. The crosslinked membrane shows hydroxide conductivity larger than 0.01 S cm^{-1} at room temperature, and the swelling by water at elevated temperature is suppressed. The H$_2$/O$_2$ AEMFC using the crosslinked membrane shows a peak power density (P_{max}) of 124.7 mW cm^{-2} at 40 °C, and the decrease of the open circuit voltage (OCV) of the fuel cell is negligible under continuous OCV conditions for 120 h. All the results indicate that the crosslinking with a macromolecular crosslinker may be a promising strategy to fabricate anion exchange membrane for the application in the AEMFCs.

1. Introduction

Proton exchange membrane fuel cells (PEMFCs) are considered to be a promising candidate for the future generation of power solutions for vehicles due to the high power density, high efficiency and low emissions [1]. However, there are still many tough problems remained in the PEMFCs, including high cost of catalysts (Pt-based catalysts), complex water and thermal management and degradation of key materials (e.g., membrane, catalysts and bipolar), which impede the large-scale commercialization of PEMFCs [2,3]. Compared with PEMFCs, numerous advantages, such as faster oxygen reduction reaction (ORR) kinetics, desirable applicability of non-precious metals as catalyst, reduced CO poisoning and milder corrosion environment [4,5], can be achieved on anion exchange membrane fuel cells (AEMFCs) which work under alkaline conditions. Therefore, increasing interests were attached to the exploitation of AEMFCs.

Anion exchange membrane (AEM), which is used to transport hydroxide from the cathode to the anode and prevent the mix of fuel and oxidant, is a key component in the AEMFC. AEMs are

* Corresponding author. Tel.: +86 411 84379153; fax: +86 411 84379185.
E-mail address: zhgshao@dicp.ac.cn (Z.-G. Shao).

usually composed of polymer matrix and anion conductive head groups. In comparison with proton exchange membrane, a higher density of conductive groups is usually required to obtain high hydroxide conductivity, because the conductivity of OH$^-$ is much lower than that of H$^+$ in aqueous phase [6]. Unfortunately, a higher conductive group density will make the membrane susceptible to swelling by water especially at elevated temperatures [7], and thus result in the decrease of mechanical strength and performance [6].

In order to resolve this problem, many strategies have been put forward to improve the hydroxide conductivity of AEMs while sustaining the dimensional and mechanical stability [6,8–11]. Therein, the so-call semi-interpenetrated polymer network (semi-IPN) was one of effective approaches. The semi-IPN was formed by combining a thermally, mechanically and chemically stable polymer with a hydroxide conducting polymer, and only one of the polymers is crosslinked [4]. Several researchers have found that semi-IPN membrane presented improved performances with good mechanical properties [11–14]. However, it would be difficult for the two polymers to distribute uniformly in the semi-IPN membrane owing to the absence of crosslinking between them, thus resulting in the phase separation of the two components and decrease of the membrane performances. For example, Lin et al. found that the hydroxide conductive poly(VBC-co-DVB) component was dispersed as spherical domains in the cardo polyetherketone matrix [14]. Although the addition of tetraethylenepentamine can form crosslinking between poly(VBC-co-DVB) and cardo polyetherketone, phase separation still took place [15]. The uneven distribution of components in the membrane perhaps explained the poor performance of AEMFC (P_{max} = 6 mW cm^{-2}) using this membrane to some extent [15].

Covalent crosslinking was another efficient technique to enhance the dimensional stability of AEMs. According to the published reports, the covalent crosslinking was mainly produced by three methods: (i) bonding halomethyl groups with aromatic rings of neighboring polymer through a Friedel−Crafts reaction without external crosslinker (self-crosslinking) [16,17], (ii) bonding two functional groups (e.g., two halomethyl groups or two tertiary amine groups) on neighboring polymer lines together in the assistance of a micromolecular crosslinker (e.g., diamines or p-Xylylenedichloride) [18,19], and (iii) bonding two polymers together by the reaction between other groups and micromolecular crosslinker [20]. The first approach mentioned above was not preferred because the crosslinking was formed at the expense of functional groups, while the other two pathways nearly all utilized micromolecular crosslinkers whose effect may be limited in comparison with a macromolecular crosslinker [21], but the later was seldom reported in the field of AEMs.

Herein, we developed a new kind of crosslinked AEMs by using a macromolecule as a crosslinker, which combines the advantages of semi-IPN and crosslinking technique. Poly(vinylbenzyl chloride) (PVBC) was used as the hydroxide conducting polymers whose chloromethyl groups could be converted to anion conductive groups, but the pure PVBC is not suitable to prepare membranes because of its high brittleness. Poly(vinyl acetal) (PVAc), synthesized through acetalization reaction between poly(vinyl alcohol) (PVA) and 4-dimethylaminobenzaldehyde (DMABA), was adopted as the macromolecular crosslinker by forming quaternary ammonium (QA) groups between dimethylamino groups on PVAc and chloromethyl groups (-CH$_2$Cl) on PVBC. Simultaneously, PVAc also played the role as the supporting matrix due to its good flexibility and film forming nature. The obtained crosslinked membranes presented high hydroxide conductivity and the membrane swelling at elevated temperature can be effectively suppressed. The P_{max} of H$_2$/O$_2$ AEMFC using the crosslinked membrane reached 124.7 mW cm^{-2} at 40 °C.

2. Experimental

2.1. Materials

PVA (degree of polymerization = 1750 ± 50) was supplied by Sinopharm Chemical Reagent Co., Ltd. (China). PVBC (60/40 mixture of 3- and 4-isomers with average molecular weight M_n = ca. 55,000 and M_w = ca. 100,000) was procured from Aldrich. 1-Methylimidazole (>99%) and DMABA came from Aladdin (China). All other chemicals with analytical grade were commercially available reagents. Moreover, all chemicals were used as received without further purification.

2.2. Synthesis of PVAc

The synthesis of PVAc was followed by the method mentioned in the literature [22]. Briefly, 4 g PVA was dissolved in 91 mL dimethyl sulphoxide (DMSO) at 50 °C, and then 6.79 g DMABA and 1.2 mL 37 wt. % HCl aqueous solution was added into the solution. After heating at 50 °C for 72 h under stirring, the product was separated by precipitation the mixture in water containing a small amount of NaOH, followed by thorough washing with de-ionized water. The polymer obtained was purified by repeated precipitations from the solution of DMSO into water, and finally dried in vacuum at 60 °C.
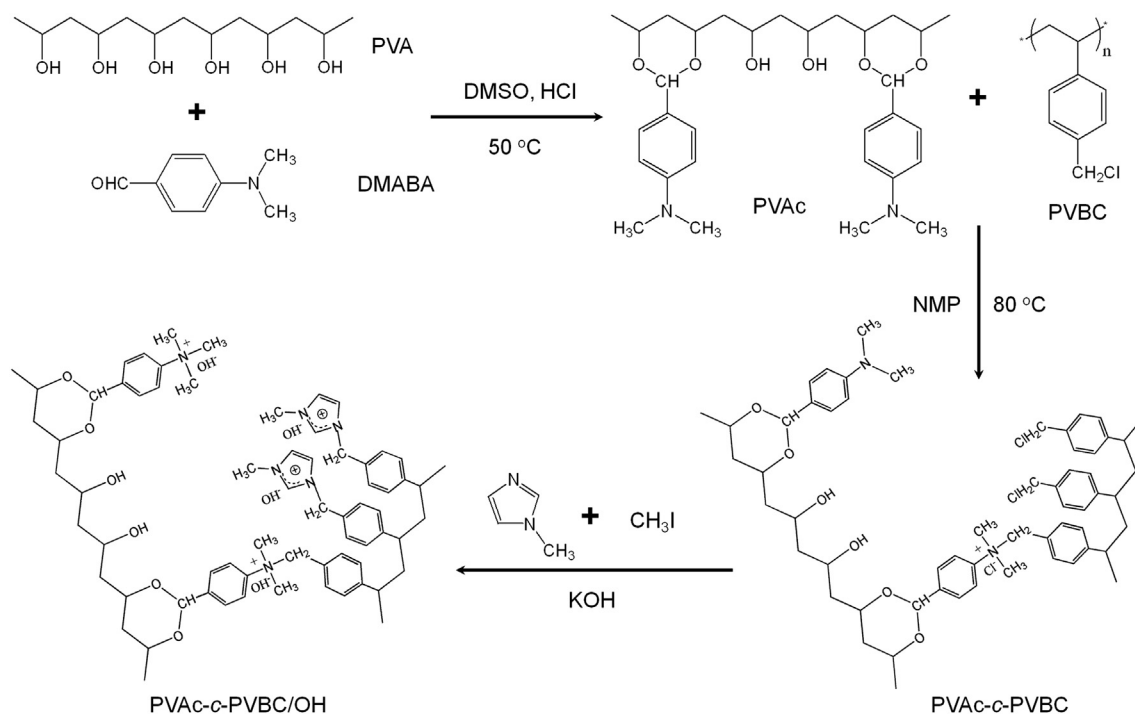
2.3. Preparation of PVAc(x)-c-PVBC(y)/OH membranes

The preparation procedure of PVBC membranes crosslinked by PVAc is shown in Scheme 1. Typically, PVAc was completely dissolved in the 1-methyl-2-pyrrolidone (NMP) to give a concentration of 0.033 g mL^{-1}. The solution containing PVBC was prepared separately by dissolving a calculated amount of PVBC in NMP. The PVAc solution was added into the PVBC solution under stirring, and the mixture was heated at 80 °C for 1 h, and then the mixture was poured onto a glass plate to cast the membrane and dried on the hot plate at 80 °C in the air. The membrane obtained was denoted as PVAc(x)-c-PVBC(y), where x:y represented the weight ratio of PVAc to PVBC. Herein, three membranes PVAc(2)-c-PVBC(1), PVAc(3)-c-PVBC(2) and PVAc(1)-c-PVBC(1) were prepared. Subsequently, the PVAc(x)-c-PVBC(y) membrane was converted to PVAc(x)-c-PVBC(y)/Cl by successively immersing in 50 vol. % 1-Methylimidazole solutions (ethanol as the solvent) for 48 h and 20 wt. % CH$_3$I solutions (ethanol as the solvent) for 24 h. After that, the membrane was immersed in a 1 M KOH aqueous solution for 24 h, converting the membranes from the Cl$^-$ form into the OH$^-$ form [PVAc(x)-c-PVBC(y)/OH], followed by washing with de-ionized water several times and storing in de-ionized water for another 36 h to remove the residual KOH prior to further experiments.

For comparison, a PVAc membrane was fabricated and immersed in a 1 M KOH aqueous solution for 24 h. After washing and storing in de-ionized water for another 36 h, the membrane obtained was denoted as PVAc/OH.

2.4. Structure characterization

The ^{1}H NMR spectroscopy was performed on a Bruker Avance II 400 NMR spectrometer at a resonance frequency of 400.13 MHz, using DMSO-d_6 as the solvent and tetramethylsilane (TMS) as an internal standard. The Fourier transform infrared (FT-IR) absorption spectra of membranes after drying at 60 °C under vacuum overnight were recorded by using a Bruker Tensor 27 spectrophotometer. The thermal properties of the membranes were tested by using a TGA analyzer (Mettler Toledo TGA/SDTA851). Before test, the membrane samples were vacuum-dried at 60 °C for 24 h. Then samples were heated from room temperature to 700 °C at a heating

Scheme 1. Preparation route of PVAc-c-PVBC/OH membranes.

rate of 10 °C min^{-1} under N$_2$ flow. Derivative thermogravimetry (DTG) curves were obtained by making the first order differential of TGA curve on temperature. The scanning electron microscope (SEM) images were taken by JEOL JSM-6360LV SEM. The elemental analysis of membrane was carried out on FEI Quanta 450 SEM equipped with Oxford Inca EDX detector. X-ray photoelectron spectra (XPS) of membranes were obtained from an ESCALAB 250Xi (Thermo Scientific) spectrometer using Al K$_\alpha$ radiation. The mechanical properties of membranes were measured on a WDW Electromechanical Universal Testing Machine (Changchun KeXin Corporation, China) at room temperature. The membrane was dried overnight before testing. The stretching test was carried out using a programmed elongation rate of 0.5 mm min^{-1}.

2.5. Ion exchange capacity, water uptake, swelling ratio and hydroxide ion conductivity

For the measurements of ion exchange capacity (IEC), water uptake (WU) and swelling ratio (SR) of PVAc(x)-c-PVBC(y)/OH membranes, the OH$^-$ form membranes were dried at 60 °C under vacuum overnight.

The IEC of membranes was determined by the back titration method. Briefly, the dried OH$^-$ form membranes were immersed in 20 mL 0.01 M HCl aqueous solutions for 24 h, followed by back titration of 0.01 M NaOH solution with phenolphthalein as the indicator. The 20 mL 0.01 M HCl solution was used as the blank sample for the control experiment. The IEC (mmol g^{-1}) of the membrane was calculated as follows:

$$IEC = \frac{(V_b - V_a)c_{HCl}}{m_{dry}} \tag{1}$$

where V_b and V_a were the consumed volumes (mL) of the NaOH solution for the blank sample and the membrane sample, respectively, c_{HCl} was the concentration of HCl solutions (mol L^{-1}), m_{dry} was the mass of dry membrane (g).

The water uptake and swelling ratio of the OH$^-$ form membranes were measured by the following equations:

$$WU = \frac{m_{wet} - m_{dry}}{m_{dry}} \tag{2}$$

$$SR = \frac{l_{wet} - l_{dry}}{l_{dry}} \tag{3}$$

where m_{wet} and m_{dry} were the mass of wet and dry membranes, respectively, l_{wet} and l_{dry} were the average length $[l_{wet} = (a_{wet} \cdot b_{wet})^{1/2}, l_{dry} = (a_{dry} \cdot b_{dry})^{1/2}]$ of wet and dry membrane samples, respectively, in which, a_{wet}, b_{wet} and a_{dry}, b_{dry} were the lengths and widths of wet and dry membrane samples, respectively.

The ionic conductivity of membrane was measured by a two-probe AC impedance spectroscopy with a Solartron 1260 frequency response analyzer (Solartron Analytical, UK) interfaced with a 1287 potentiostat/galvanostat. The measurement was conducted in the potentiostatic mode over frequencies ranging from 1 MHz to 1 Hz with a potentiostatically controlled AC potential of 10 mV. Ionic conductivity, σ (S cm^{-1}), was calculated according to the following equation:

$$\sigma = l/wdR \tag{4}$$

where l was the length of the membrane (cm) between two electrode, w and d was the membrane width and thickness (cm), respectively, R was the measured membrane resistance (Ω).

2.6. Alkaline and oxidative stability testing

The alkaline stability of PVAc(x)-c-PVBC(y)/OH membranes was evaluated by monitoring the variation of conductivity in 1 M KOH at 40 °C. After a given time, the membrane was taken out and the

residual KOH was removed, and then its hydroxide conductivity at room temperature was measured by the method mentioned above.

The oxidative stability of PVAc(x)-c-PVBC(y)/OH membranes was studied by estimating the weight of the membrane in Fenton's reagent. A piece of the membrane was immersed into Fenton's reagent (4×10^{-6} mol L^{-1} FeSO$_4$ in 3% H$_2$O$_2$) at 40 °C. The membrane was taken out of the solution after a given time, weighed after removing the surface liquid with filter paper and put into the Fenton's reagent again.

2.7. H$_2$/O$_2$ fuel cell testing

The gas diffusion electrode (GDE) was fabricated as follows: The catalyst ink was prepared by ultrasonically blending 70 wt. % Pt/C (Johnson Matthey) electrocatalysts powder with AS-4 ionomer (Tokayama, Japan) and isopropanol for 30 min. The weight ratio of catalyst to ionomer was 8:2. The catalyst ink was then sprayed onto a wet-proofed carbon gas diffusion layer (GDL) on the hot plate at 50 °C. The Pt loading for all electrodes was 0.4 mg$_{Pt}$ cm^{-2}.

The water on the surface of PVAc(1)-c-PVBC(1)/OH membrane (45–50 μm in thickness) was absorbed by filter papers before use. The MEAs with an active area of 2 cm^2 were fabricated by hot-pressing the anode and cathode electrodes on both sides of a PVAc(1)-c-PVBC(1)/OH membrane at 60 °C for 2 min. The MEA was then cooled and assembled in single cells for testing.

The fuel cell was tested at 40 °C with fully humidified H$_2$ and O$_2$ under 0.05 MPa (back pressure) for the anode and cathode, respectively. The flow rate for H$_2$ and O$_2$ was 40 and 70 mL min^{-1}, respectively. The polarization curve was measured by Kikusui PLZ-50F electronic load. The stability of fuel cell under constant current was carried out at 100 mA cm^{-2}, during which the cell voltage was monitored. Moreover, the oxidative stability of membrane was tested under continuous OCV conditions. After holding at OCV for some time, the cell was discharged at 0.1 V for 1–2 h, and then the OCV was recorded.

3. Results and discussion

3.1. Structure characterization

Under the catalysis of HCl, two hydroxyl groups of PVA can react with the aldehyde group of DMABA, and PVAc was obtained

(Scheme 1). The ^{1}H NMR spectra of PVA and PVAc are shown in Fig. 1. Compared with PVA, several new peaks appeared on the spectrum of PVAc. The two peaks at 7.20 ppm and 6.65 ppm were ascribed to the hydrogen atoms of benzene ring (marked as d), and the peaks at 5.38 ppm and 3.34 ppm can be attributed to the hydrogen atoms of −CH− (marked as c) and methyl (marked as e), respectively [22]. The FT-IR spectra of PVA and PVAc are presented in Fig. 2. The spectrum of PVA is consistent with that reported in the literature, i.e., the broad band from 3250 to 3550 cm^{-1} is from the hydroxyl groups of PVA or the possibly bonded water, the bands at 2906 and 2941 cm^{-1} come from the asymmetrical and symmetrical stretching of C−H in the PVA backbone, the two peaks at 1423 and 1330 cm^{-1} are ascribed to the secondary O−H in-plane bending and C−H wagging vibrations, the C−C−C stretching band is presented at 1143 cm^{-1}, and the band centered at 1093 cm^{-1} represents the C−O stretching vibration of PVA [23]. In comparison with PVA, there are two new peaks centered at 1527 and 1618 cm^{-1} appearing in the spectrum of PVAc, which can be attributed to the C=C of aromatic hydrocarbon [18]. The difference in the ^{1}H NMR and FT-IR spectra definitely confirmed the successful introduction of dimethylamino groups to PVA.

The PVAc was used as a macromolecular crosslinker to interconnect with PVBC by forming QA groups between dimethylamino groups and −CH$_2$Cl groups. The mixture of PVAc and PVBC in NMP was heated at 80 °C to initiate the reaction between dimethylamino groups and −CH$_2$Cl groups. Long heating time should be avoided, because it was found that gelation took place after 75 min. As a result, 60 min was adopted to transform some amount of −CH$_2$Cl groups in solution. Subsequently, the mixture was poured onto a glass plate and heated at 80 °C to evaporate the solvent, during which some other dimethylamino groups will react with −CH$_2$Cl groups (Scheme 1). After the remove of solvent, the PVAc(x)-c-PVBC(y) membrane can be obtained, which was formed by the crosslinking between PVAc and PVBC. As shown in Fig. 3, both PVAc(x)-c-PVBC(y) and PVAc membranes are transparent, but the color of PVAc(x)-c-PVBC(y) membrane is slight yellow, while the PVAc membrane is colorless. In the FT-IR spectrum of PVAc(1)-c-PVBC(1), the absorption bands at 675, 709 and 1267 cm^{-1} arise from stretching vibrations of unreacted −CH$_2$Cl groups [24,25], while the peak at 1672 cm^{-1} can be ascribed to the QA groups [10]. Moreover, XPS was employed to identify the change of groups in the preparation of membrane. As shown in Fig. 4, only one peak
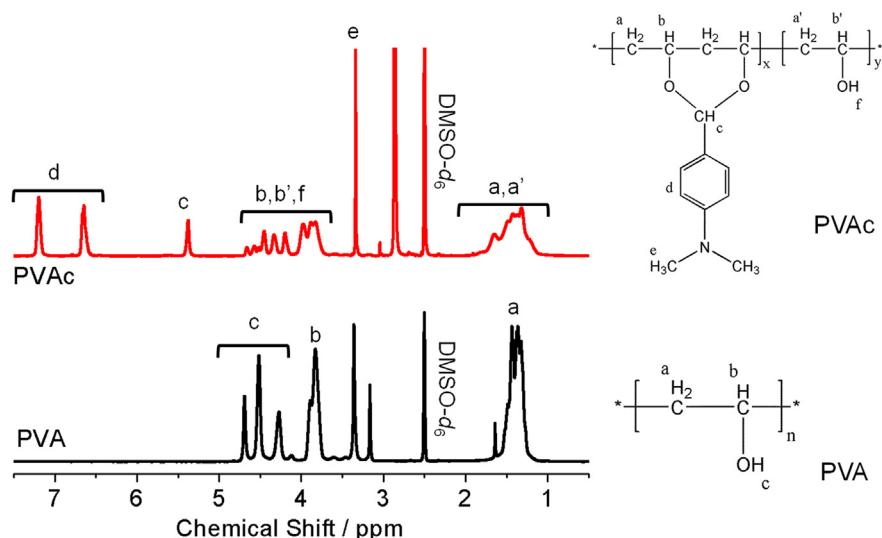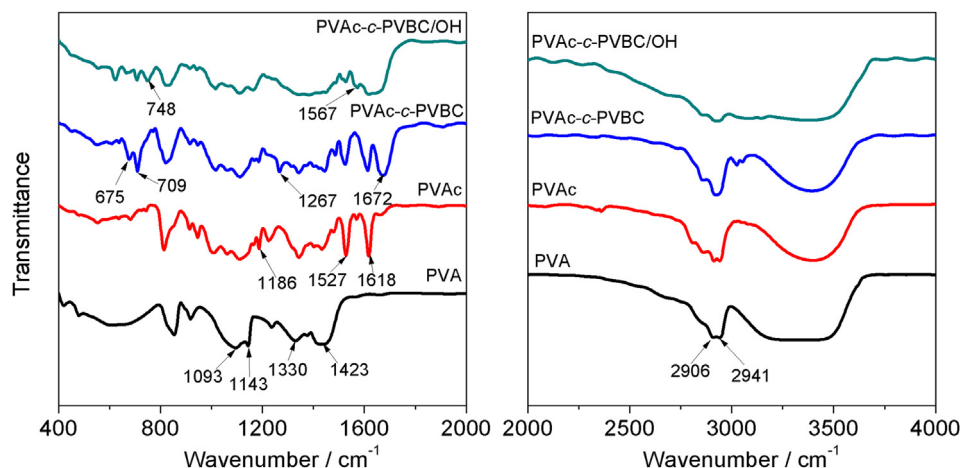

Fig. 1. ^{1}H NMR spectra of PVA and PVAc.

Fig. 2. FT-IR spectra of different membranes.

(locating at 399.8 eV) is found in the N 1s spectrum of PVAc, and this peak comes from the tertiary amino groups of PVAc [8]. For PVAc(1)-c-PVBC(1) membrane, a new peak emerges at 402.1 eV, which can be ascribed to the QA groups [8]. The above results definitely indicated that the crosslinked PVBC membrane with macromolecular crosslinker has been successfully prepared.

After treating with 1-methylimidazole and CH3I, the remaining dimethylamino and −CH2Cl groups were converted to QA and imidazolium groups, respectively, resulting in PVAc(x)-c-PVBC(y)/Cl membrane, which can be further transformed to OH⁻ form membrane [PVAc(x)-c-PVBC(y)/OH] by alkalization with KOH (Scheme 1). As shown in Fig. 2, the absorption bands representing −CH2Cl groups disappeared in the FT-IR spectrum of PVAc(1)-c-

PVBC(1)/OH, whereas two new peaks at 748 and 1567 cm⁻¹ arose, which can be attributed to the vibrational mode of imidazolium cations [26]. Moreover, the elemental analysis revealed that the chloride elements in the PVAc(1)-c-PVBC(1) completely disappeared in the PVAc(1)-c-PVBC(1)/OH membrane (Figs. 5a and 6a), further proving the sufficient conversion of −CH2Cl groups.

One critical concern about AEM with two components is related to phase separation. Fortunately, no phase separation was found in the resulting PVAc(x)-c-PVBC(y) or PVAc(x)-c-PVBC(y)/OH membranes. We took PVAc(1)-c-PVBC(1) membrane for example. First, the PVAc(1)-c-PVBC(1) membrane was transparent, uniform and homogeneous in the photograph (Fig. 3b). Second, in the EDX spectrum of PVAc(1)-c-PVBC(1) membrane, the Cl and O element were distributed uniformly throughout the whole range of the membrane (Fig. 5b−e). Third, the PVAc(1)-c-PVBC(1)/OH membrane was compact, uniform and homogeneous at a magnification of 3000 and 10,000 in the SEM images (Fig. 6b−d), while obvious phase separation between the two components of the semi-IPN membranes reported previously [14,15] could be easily observed by SEM measurement.

It was considered that the formation of homogeneous membrane might be caused by the close connection between PVAc and PVBC molecular chains through crosslinking. As a result, in order to verify this assumption, a hybrid membrane consisting of PVA and PVBC was prepared by the same method with PVAc-c-PVBC, except that PVAc was replaced by PVA. In this case, there will be no crosslinking between the two components (i.e., PVA and PVBC). The
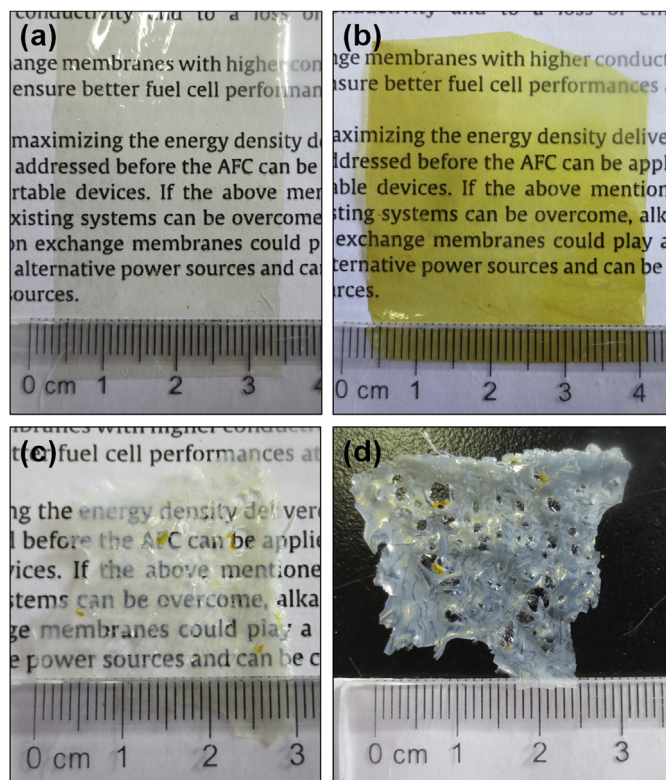

Fig. 3. Photographs of (a) PVAc membrane, (b) PVAc(1)-c-PVBC(1) membrane and (c, d) membrane made by blending PVA and PVBC with the weight ratio of PVA/PVBC = 1 on different substrate.
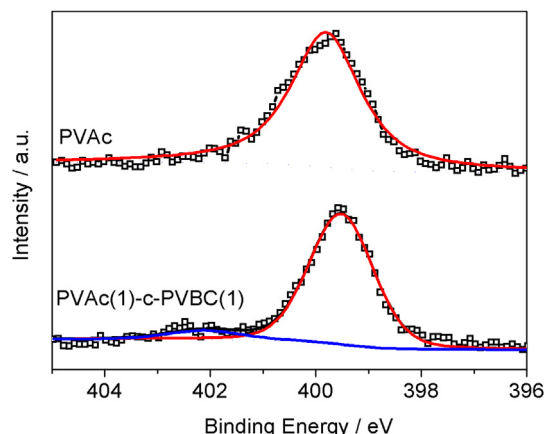

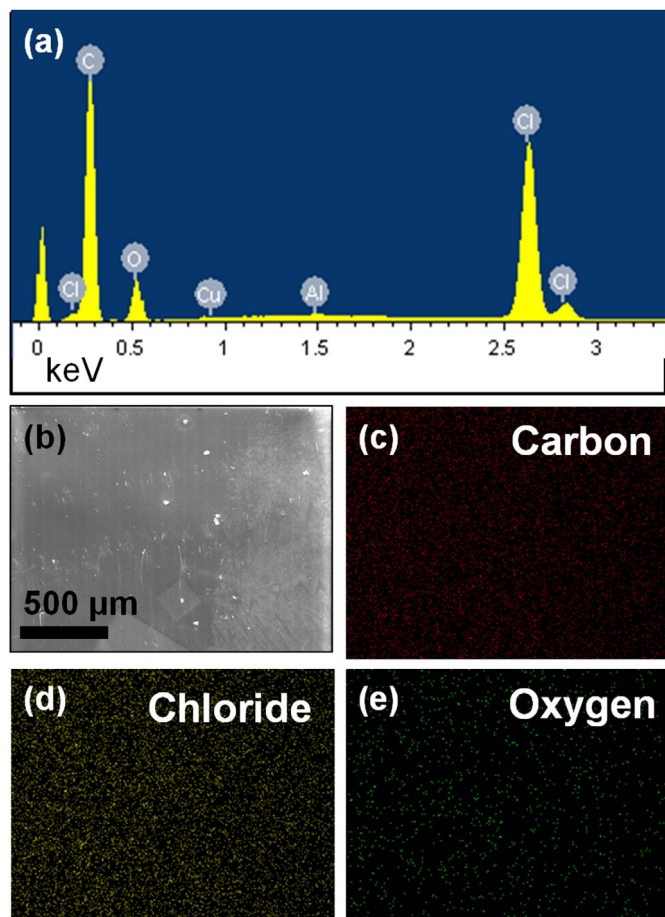**Fig. 4.** XPS spectra of PVAc and PVAc(1)-c-PVBC(1) membranes.

Fig. 5. (a) EDX spectrum of the PVAc(1)-c-PVBC(1) membrane. (b—e) The compositional mapping images of the PVAc(1)-c-PVBC(1) membrane.

obtained PVA-PVBC hybrid membrane was translucent and remarkably nonuniform with holes in appearance (Fig. 3c and d). Additionally, the hybrid membrane was very brittle and broke into pieces easily. Although PVA had good flexibility and film forming nature, the hybrid PVA—PVBC membrane was quite poor in mechanical properties, which may be caused by the weak interaction between PVA and PVBC molecular chains. The above results indicated that the crosslinking played an important role in the formation of homogeneous and uniform membranes. The excellent compactness and homogeneity of the PVAc(1)-c-PVBC(1)/OH is beneficial for the fuel cell application because the gas-impermeability is required.

The thermal degradation of polymers was investigated using thermogravimetric (TG) analysis between room temperature and 700 °C under N_2 protection. The first weight loss of PVA starts at 210 °C due to the degradation of hydroxyl groups and the second weight loss stage starting above 400 °C is attributed to the splitting of the main chain (line 1 in Fig. 7). When the acetal groups were introduced to the PVA, the first weight lost peak was delayed from ~250 °C to ~310 °C, suggesting the better thermal stability of acetal groups (line 3 in Fig. 7). The curve for PVBC shows two weight loss steps (line 2 in Fig. 7): −CH₂Cl groups degradation starting from 350 °C and main-chain decomposition taking place above 450 °C. As for the PVAc(1)-c-PVBC(1) (line 4 in Fig. 7), a new weight loss step starts at ~150 °C, which can be ascribed to the degradation of QA groups. In the weight loss curve of PVAc(1)-PVBC(1)/OH (line 5 in Fig. 7), the weight loss before 220 °C can be attributed to the elimination of bonded water and residual

solvent (<130 °C) followed by the decomposition of QA groups. The weight loss step initiating at 230 °C results from the degradation of imidazolium cations, which is close to the degradation temperature of imidazolium cations reported in the literature [27,28] and larger than that of QA groups [7,29,30].

The mechanical properties of membranes were shown in Table 1. The PVAc/OH membrane has tensile strength at maximum load of 19.4 MPa and an elongation at break of 14.8%. After crosslinking, the PVAc(x)-c-PVBC(y)/OH membranes showed tensile strength in the range of 14—18 MPa and elongation at break between 5% and 12%. The tensile strength and elongation at break for the PVAc(x)-c-PVBC(y)/OH membranes are close to the methylated melamine crosslinked PVBC membrane [31] and semi-IPN structured Poly(VBC-co-DVB) + PEK-C + TEPA membrane [15].

3.2. IEC, water uptake, swelling ratio, hydroxide conductivity and stability of PVAc(x)-c-PVBC(y)/OH membrane

Three AEMs with different weight ratio of PVAc to PVBC were prepared and their properties are listed in Table 1. With the increase of the content of PVBC, the IEC of PVAc(x)-c-PVBC(y)/OH membrane increases. Correspondingly, the WU, SR and hydroxide conductivity of the membrane also increased, which is consistent with the common regularity of AEMs. The temperature dependence of WU and SR is shown in Fig. 8. It can be found that the WU and SR nearly do not increase with the growth of temperature, i.e., the swelling of AEMs is inhibited by the crosslinking, which is positive for the application under elevated temperature. The hydroxide conductivities at room temperature of the three PVAc(x)-c-PVBC(y)/OH membranes were all larger than 0.01 S cm^{-1} (Table 1), indicating that PVAc(x)-c-PVBC(y)/OH membrane meet the conductivity requirement of AEMFCs [6]. Similarly, the hydroxide conductivity of AEMs increases with the rise of temperature, reaching 0.026, 0.041 and 0.054 S cm^{-1} at 80 °C for the PVAc(2)-c-PVBC(1)/OH, PVAc(3)-c-PVBC(2)/OH and PVAc(1)-c-PVBC(1)/OH membrane, respectively (Fig. 9). It was reported that the KOH doped PVA membrane also showed a little conductivity towards hydroxide [32], so the PVAc membrane treated with KOH (PVAc/OH) was prepared to evaluate the contribution of PVAc to the conduction of hydroxide in the crosslinked membrane. As shown in Table 1, the IEC, WU and SR of the PVAc/OH membrane were much smaller than those of PVAc(x)-c-PVBC(y)/OH membranes, and the conductivity of PVAc/OH was too low to be measured accurately. As a result, it can be concluded that the conductivity of the PVAc(x)-c-PVBC(y)/OH membrane mainly come from the PVBC component. The PVAc(x)-c-PVBC(y)/OH membranes developed in this work presented good conductivity, but the WU and SR seemed larger than the desired values. The high WU and SR might be caused by the hydroxyl groups in the PVAc, resulting in the hydrophilic nature of the matrix of PVAc(x)-c-PVBC(y) membrane. Recently, it was supposed that producing hydrophilic/hydrophobic micro-phase separation structure in the membrane would increase the hydroxide conductivity of membrane with relatively low WU and SR [6,9,33]. As a result, replacing PVAc with a more hydrophobic polymer could decrease the WU and SR of the membrane, and the hydroxide conductivity was expected to be improved by the formation of hydrophilic/hydrophobic micro-phase separation. The corresponding investigation is underway.

The chemical resistance of AEMs to alkaline and oxidative environments is an important index in the development of AEMs. In this study, the alkaline stability of PVAc(2)-c-PVBC(1)/OH, PVAc(3)-c-PVBC(2)/OH and PVAc(1)-c-PVBC(1)/OH was evaluated by monitoring the hydroxide conductivity (room temperature) in 1 M KOH at 40 °C. As shown in Fig. 10, the hydroxide conductivities of AEMs decline gradually with the exposing time in 1 M KOH, and the
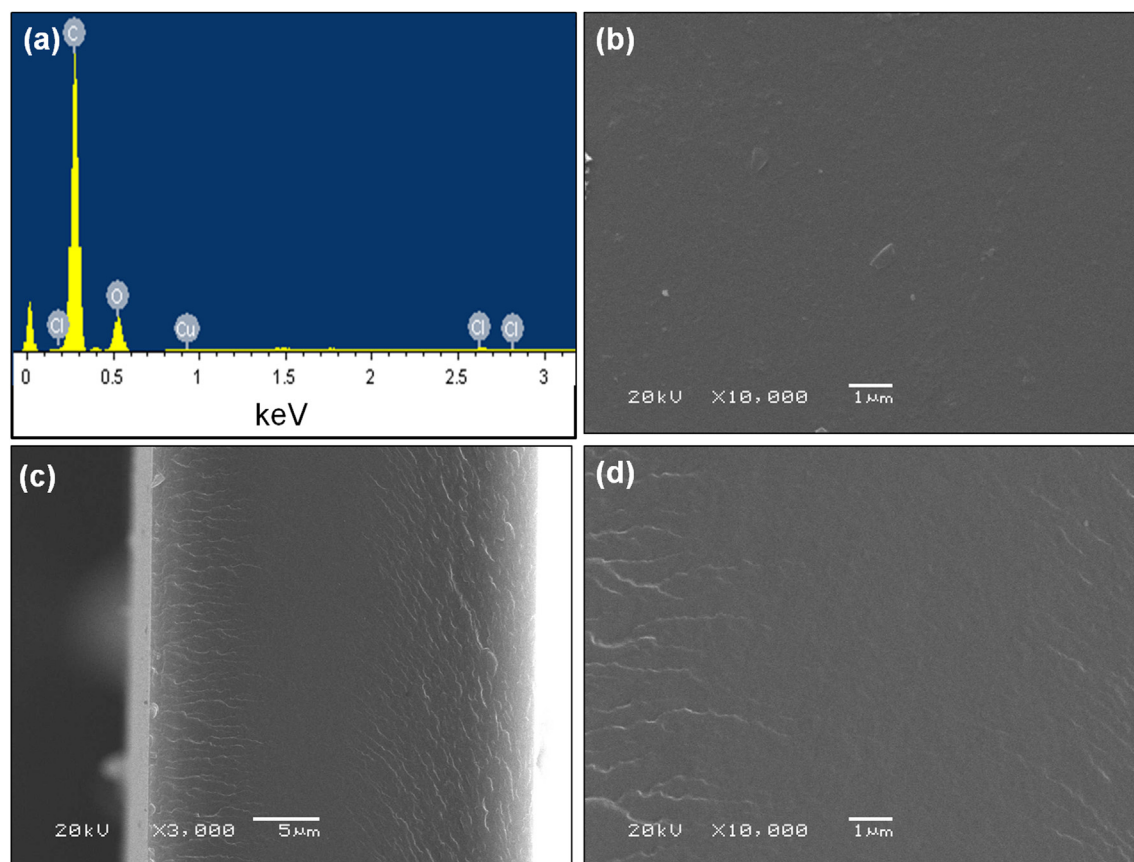
Fig. 6. (a) EDX spectrum of the PVAc(1)-c-PVBC(1)/OH membrane; (b–d) SEM images of surface (b) and cross-section (c, d) of PVAc(1)-c-PVBC(1)/OH membrane at different magnifications.

hydroxide conductivity loss was more remarkable for the membrane with higher IEC. The decline of the hydroxide conductivity of PVAc(x)-c-PVBC(y)/OH probably resulted from the degradation of imidazolium groups by the attack of OH⁻, which has been observed by many researchers in the investigation of imidazolium-based AEMs [5,34,35]. Recently, it was reported that crowding around the reactive C2 position of the imidazolium group by installation of adjacent bulky groups would hinder nucleophilic attack by OH⁻, thus improving the stability of the imidazolium group [36], which gave us a pathway in the future work to improve the stability of conductive groups of AEM.

The oxidative stability of the three membranes was estimated by monitoring the mass loss of membrane sample in the Fenton's reagent. This method is commonly used in the accelerated durability test of proton exchange membrane for PEMFCs [37,38], and it is now also adopted in the development of AEMs [25,39]. As shown in Fig. 11, the mass of the membrane gradually lost with the immersing time in the Fenton's reagent, but none of them was dissolved after more than 200 h, indicating the acceptable stability. In addition, the IEC of PVAc(2)-c-PVBC(1)/OH, PVAc(3)-c-PVBC(2)/OH and PVAc(1)-c-PVBC(1)/OH membrane after degradation was 0.54, 0.74 and 0.77 mmol g⁻¹, respectively, suggesting the degradation of ion conductive groups induced by Fenton's reagent.

3.3. Fuel cell testing

Owing to the highest hydroxide conductivity, the PVAc(1)-c-PVBC(1)/OH membrane (45–50 μm in thickness) was used for the single cell testing. The performance of the fuel cell was evaluated at 40 °C with fully humidified H₂/O₂ under 0.05 MPa (back pressure).

As shown in Fig. 12, the OCV of the AEMFC is 1.035 V, indicating good gas barrier property of the membrane, and a P_{max} of 124.7 mW cm⁻² is obtained at 0.399 V, which is obviously larger than the P_{max} of 48 mW cm⁻² [18] and 80 mW cm⁻² [11] reported previously using crosslinked AEM and semi-IPN AEM in the fuel cell, respectively, and it is also larger than the P_{max} of 30 mW cm⁻² presented by the AEMFC applying imidazolium-based AEM [34].
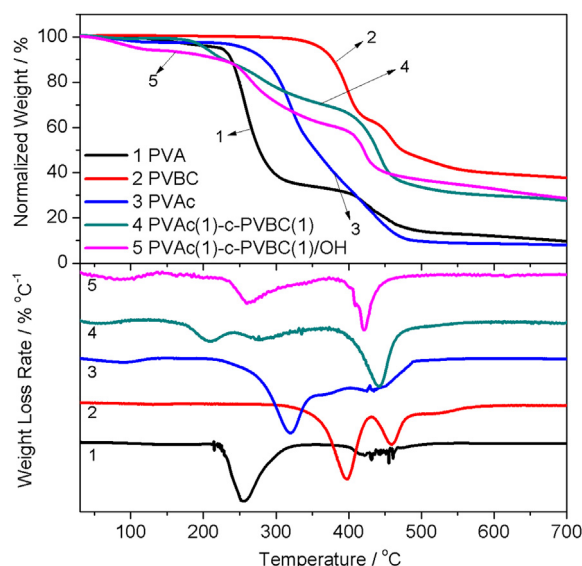

Fig. 7. TGA and DTG curves of different membranes.

Table 1
IEC, water uptake, swelling ratio, hydroxide conductivity and mechanical properties of PVAc/OH and PVAc(x)-c-PVBC(y)/OH membranes.

Membrane samples	IEC mmol g^{-1}	WU[a] %	SR[a] %	σ[a] S cm^{-1}	Tensile strength[b] MPa	Elongation at break[b] %
PVAc/OH	0.14	11.0	3.7	n.a.[c]	19.4	14.8
PVAc(2)-c-PVBC(1)/OH	0.85	69.5	17.4	0.014	15.7	5.6
PVAc(3)-c-PVBC(2)/OH	1.05	81.4	20.1	0.023	17.2	9.3
PVAc(1)-c-PVBC(1)/OH	1.26	139.1	26.3	0.029	14.2	11.7

[a] Measured at room temperature.
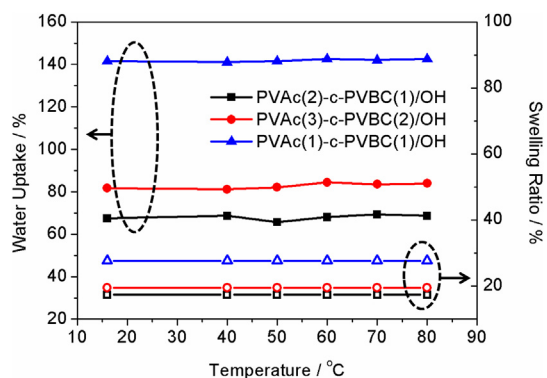[b] Measured in the dry state.
[c] Cannot be measured accurately.

Fig. 8. Water uptake and swelling ratio of membranes at different temperature.

Fig. 10. Hydroxide conductivity loss for PVAc(x)-c-PVBC(y)/OH membranes as a function of time in 1 M KOH at 40 °C.

Fig. 11. Weight loss of PVAc(x)-c-PVBC(y)/OH membranes in Fenton's reagent at 40 °C.

The detailed comparison of the fuel cell performances in this work and literature is listed in Table 2. The high power output ability demonstrated the outstanding performances of the PVAc(1)-c-PVBC(1)/OH membrane. It is necessary to be pointed out that the fuel cell performance was influenced significantly by the architectures of catalyst layer, fabrication method of MEA and operating conditions [10,31,40]. As a result, great efforts should be focused on these issues in addition to improving the performance of AEMs.

The durability is of great importance in the development of AEMs. Herein, the durability of PVAc(1)-c-PVBC(1)/OH membrane was evaluated under constant current and OCV conditions, respectively. Fig. 13 shows the cell voltage variation under constant current of 100 mA cm^{-2}. It can be seen that the voltage declines rapidly in the first 240 min (4 h), and the decrease trend is relatively
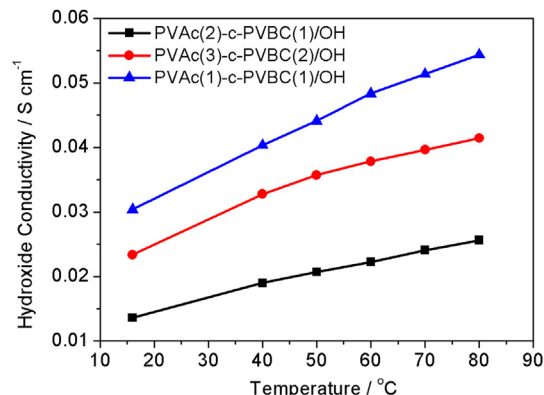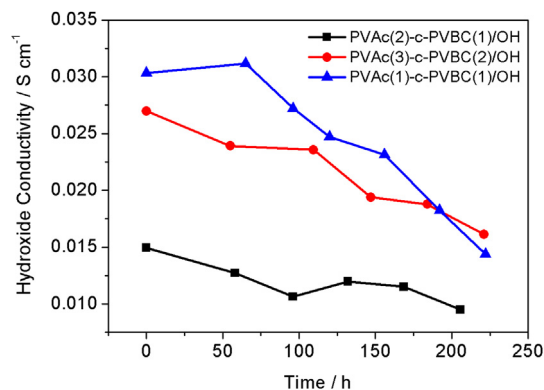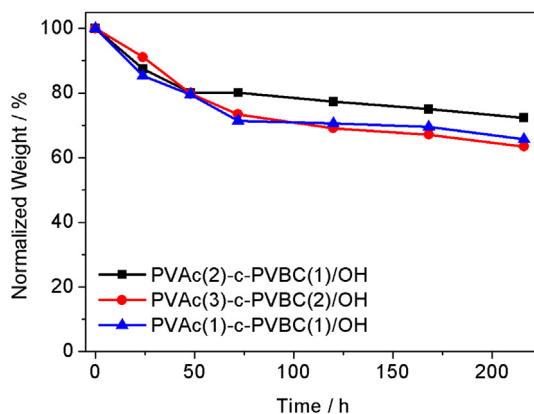
flat in the subsequent 1200 min (20 h). Presently, the durability under working conditions is one of the severest shortcomings of AEMs. For example, the decline of voltage is nearly 300 mV during 1440 min at constant current for the fuel cell using quaternized poly-[(methyl methacrylate)-co-(butyl acrylate)-co-(vinylbenzyl chloride)] membrane [29]. Additionally, for the recent reported AEMFC using a crosslinked membrane, the current density cannot remain stable and ca. 30% loss was observed after only 140 min [15]. The reasons for the performance reduction of AEMFC are unclear at present. Lowering the water uptake and increasing the mechanical strength of the membrane may be able to improve the durability of
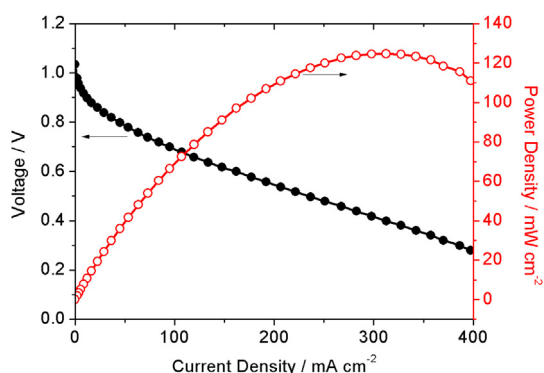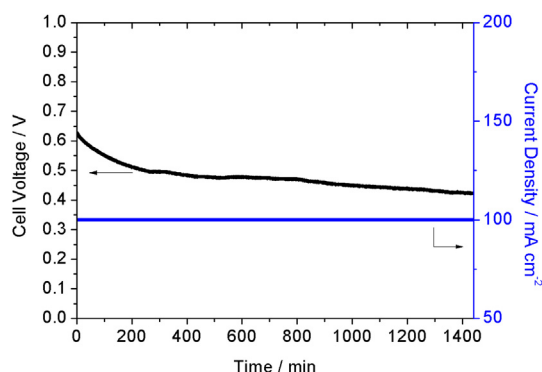

Fig. 9. Hydroxide conductivities of membranes at different temperature.

Fig. 12. Polarization and power density curves of H$_2$/O$_2$ fuel cell with PVAc(1)-c-PVBC(1)/OH membrane at 40 °C.
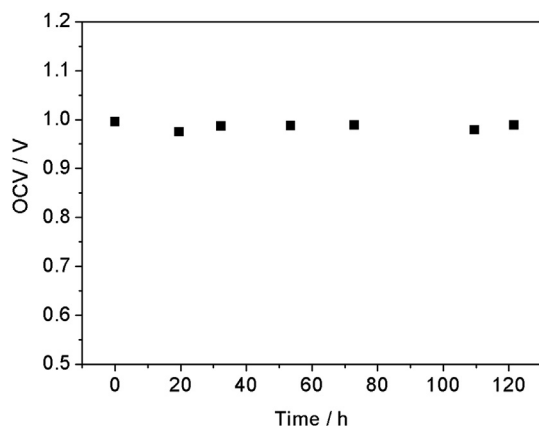
Table 2
Comparison of the single AEMFC performance in this work and literature (the electrodes used are all GDE-type).

AEM	Thickness μm	Pt loading $mg_{Pt}\ cm^{-2}$	Ionomer	Temperature/back pressure °C/MPa	P_{max} mW cm^{-2}	Reference
PVAc(1)-c-PVBC(1)/OH	45–50 (wet)	0.4	AS-4	40/0.05	124.7	This work
QPMV-PDVB (semi-IPN)	n.a.	0.4 ± 0.05	QPMBV	70/0.1	80	[11]
Crosslinked ETFE-g-VBC	n.a.	0.8[a]	Imidazolium-based ionomer	40/0	48	[18]
Poly(VBC-co-DVB) + PEK-C + TEPA	n.a.	0.4	PVBC crosslinked by TMHDA	50/0	6	[15]
QAPS	30 (dry)	0.4	AS-4	50/0.05	145	[10]
FAA-3	50–55	0.5	FAA-3	40/0	41	[40]
OBuTMA–AAEPs-1.0	40–60	0.4	PVBC crosslinked by TMHDA	50/n.a.	120	[41]
Imidazolium-based PPO	n.a.	0.4	PVBC crosslinked by TMHDA	50/0	30	[34]

[a] Calculated from the catalyst loading and Pt content of the catalyst.

Fig. 13. Durability test of H_2/O_2 fuel cell with PVAc(1)-c-PVBC(1)/OH membrane at 40 °C. The current density of the fuel cell was controlled at 100 mA cm^{-2}.

fuel cell [29]. Besides, the change of three-phase boundaries in the catalyst layer might be another cause for the degradation of AEMFC. Large amount of work are still needed to investigate the degradation of AEMFC in detail.

Furthermore, the stability of AEM was evaluated under oxidative conditions (continuous OCV conditions), which is also a commonly used method for the testing of oxidative stability of polymer electrolyte membrane of fuel cells. As shown in Fig. 14, the OCV of the fuel cell is above 0.99 V throughout the whole testing period (120 h), indicating good tolerance to oxidative environments for the PVAc(1)-c-PVBC(1)/OH membrane.

Fig. 14. Open circuit voltage of fuel cell with PVAc(1)-c-PVBC(1)/OH membrane as a function of time under humidified H_2/O_2 at 40 °C.

4. Conclusions

A new kind of crosslinked AEMs by using a macromolecule as a crosslinker was developed, which combined the advantages of semi-IPN and crosslinking technique. PVBC was utilized as the hydroxide conducting polymers, while PVAc containing dimethylamino groups was adopted as the macromolecular crosslinker and the supporting matrix simultaneously. The macromolecular polymer and dimethylamino groups were two important factors to obtain homogeneous and flexible crosslinked PVBC membranes. Thanks to the crosslinking, the swelling by water at elevated temperature was suppressed for the resulting membrane. The crosslinked membrane presented high conductivity for hydroxide and superior performances in the single fuel cell testing. All the results indicated that the crosslinking with a macromolecular crosslinker may be a promising strategy to fabricate AEMs for the application in the AEMFCs. Future work should be focused on increasing the mechanical strength of the membrane and improving the stability of the anion conductive groups.

References

[1] Y. Wang, K.S. Chen, J. Mishler, S.C. Cho, X.C. Adroher, Appl. Energy 88 (2011) 981–1007.
[2] U.S. DOE, http://www1.eere.energy.gov/hydrogenandfuelcells/mypp/pdfs/fuel_cells.pdf, 2011.
[3] Y.H. Bing, H.S. Liu, L. Zhang, D. Ghosh, J.J. Zhang, Chem. Soc. Rev. 39 (2010) 2184–2202.
[4] G. Couture, A. Alaaeddine, F. Boschet, B. Ameduri, Prog. Polym. Sci. 36 (2011) 1521–1557.
[5] O.I. Deavin, S. Murphy, A.L. Ong, S.D. Poynton, R. Zeng, H. Herman, J.R. Varcoe, Energy Environ. Sci. 5 (2012) 8584–8597.
[6] J. Pan, C. Chen, L. Zhuang, J.T. Lu, Acc. Chem. Res. 45 (2012) 473–481.
[7] X. Yan, G. He, S. Gu, X. Wu, L. Du, H. Zhang, J. Membr. Sci. 375 (2011) 204–211.
[8] J. Pan, Y. Li, L. Zhuang, J. Lu, Chem. Commun. 46 (2010) 8597–8599.
[9] N. Li, T. Yan, Z. Li, T. Thurn-Albrecht, W.H. Binder, Energy Environ. Sci. 5 (2012) 7888–7892.
[10] Y. Zhao, J. Pan, H. Yu, D. Yang, J. Li, L. Zhuang, Z. Shao, B. Yi, Int. J. Hydrogen Energy 38 (2013) 1983–1987.
[11] Y. Luo, J. Guo, C. Wang, D. Chu, Electrochem. Commun. 16 (2012) 65–68.
[12] M. Kumar, S. Singh, V.K. Shahi, J. Phys. Chem. B 114 (2010) 198–206.
[13] J.L. Wang, R.H. He, Q.T. Che, J. Colloid Interface Sci. 361 (2011) 219–225.
[14] X. Lin, M. Gong, Y. Liu, L. Wu, Y. Li, X. Liang, Q. Li, T. Xu, J. Membr. Sci. 425–426 (2013) 190–199.
[15] X. Lin, Y. Liu, S.D. Poynton, A.L. Ong, J.R. Varcoe, L. Wu, Y. Li, X. Liang, Q. Li, T. Xu, J. Power Sources 233 (2013) 259–268.
[16] S. Gu, R. Cai, Y.S. Yan, Chem. Commun. 47 (2011) 2856–2858.

[17] H. Sun, G. Zhang, Z. Liu, N. Zhang, L. Zhang, W. Ma, C. Zhao, D. Qi, G. Li, H. Na, Int. J. Hydrogen Energy 37 (2012) 9873—9881.

[18] J. Fang, Y. Yang, X. Lu, M. Ye, W. Li, Y. Zhang, Int. J. Hydrogen Energy 37 (2012) 594—602.

[19] E.N. Komkova, D.F. Stamatialis, H. Strathmann, M. Wessling, J. Membr. Sci. 244 (2004) 25—34.

[20] J.F. Zhou, M. Unlu, I. Anestis-Richard, P.A. Kohl, J. Membr. Sci. 350 (2010) 286—292.

[21] G. Zhang, H. Li, W. Ma, L. Zhang, C.M. Lew, D. Xu, M. Han, Y. Zhang, J. Wu, H. Na, J. Mater. Chem. 21 (2011) 5511—5518.

[22] V.D. Toncheva, S.D. Ivanova, R.S. Velichkova, Eur. Polym. J. 30 (1994) 741—747.

[23] Y. Zhang, P.C. Zhu, D. Edgren, J. Polym. Res. 17 (2010) 725—730.

[24] J.H. Wang, S.H. Li, S.B. Zhang, Macromolecules 43 (2010) 3890—3896.

[25] Y.M. Zhang, J. Fang, Y.B. Wu, H.K. Xu, X.J. Chi, W. Li, Y.X. Yang, G. Yan, Y.Z. Zhuang, J. Colloid Interface Sci. 381 (2012) 59—66.

[26] B.C. Lin, L.H. Qiu, J.M. Lu, F. Yan, Chem. Mater. 22 (2010) 6718—6725.

[27] X. Yan, G. He, S. Gu, X. Wu, L. Du, Y. Wang, Int. J. Hydrogen Energy (2012) 5216—5224.

[28] A.H.N. Rao, R.L. Thankamony, H.-J. Kim, S. Nam, T.-H. Kim, Polymer 54 (2013) 111—119.

[29] Y.T. Luo, J.C. Guo, C.S. Wang, D. Chu, Macromol. Chem. Phys. 212 (2011) 2094—2102.

[30] Z. Zhao, F. Gong, S. Zhang, S. Li, J. Power Sources 218 (2012) 368—374.

[31] Y.-C. Cao, X. Wang, M. Mamlouk, K. Scott, J. Mater. Chem. 21 (2011) 12910—12916.

[32] J. Qiao, J. Fu, R. Lin, J. Ma, J. Liu, Polymer 51 (2010) 4850—4859.

[33] M. Tanaka, K. Fukasawa, E. Nishino, S. Yamaguchi, K. Yamada, H. Tanaka, B. Bae, K. Miyatake, M. Watanabe, J. Am. Chem. Soc. 133 (2011) 10646—10654.

[34] J. Ran, L. Wu, J.R. Varcoe, A.L. Ong, S.D. Poynton, T. Xu, J. Membr. Sci. 415—416 (2012) 242—249.

[35] Y.S. Ye, Y.A. Elabd, Macromolecules 44 (2011) 8494—8503.

[36] O.D. Thomas, K.J.W.Y. Soo, T.J. Peckham, M.P. Kulkarni, S. Holdcroft, J. Am. Chem. Soc. 134 (2012) 10753—10756.

[37] D. Zhao, B.L. Yi, H.M. Zhang, M.L. Liu, J. Power Sources 195 (2010) 4606—4612.

[38] D. Zhao, J.H. Li, M.K. Song, B.L. Yi, H.M. Zhang, M.L. Liu, Adv. Energy Mater. 1 (2011) 203—211.

[39] K. Shen, J. Pang, S. Feng, Y. Wang, Z. Jiang, J. Membr. Sci. (2013) 20—28.

[40] M. Carmo, G. Doubek, R.C. Sekol, M. Linardi, A.D. Taylor, J. Power Sources 230 (2013) 169—175.

[41] Z. Zhang, L. Wu, J. Varcoe, C. Li, A.L. Ong, S. Poynton, T. Xu, J. Mater. Chem. A 1 (2013) 2595—2601.